Desalination and Water Treatment
www.deswater.com

doi: 10.5004/dwt.2018.21807

112 (2018) 171–178
April

Understanding of photosynthetically active radiation index under soil salinity variation using remote sensing practices in arid environments

Mohamed Elhag

Department of Hydrology and Water Resources Management, Faculty of Meteorology, Environment and Arid Land Agriculture, King Abdulaziz University, Jeddah 21589, Saudi Arabia, email: melhag@kau.edu.sa

Received 2 August 2017; Accepted 14 December 2017

ABSTRACT

Soil salinity is the key factor limiting agricultural expansion over poorly drained soils. In Saudi Arabia, the main source of irrigational water is the groundwater aquifers. Therefore, groundwater resources are under constant pressure and over exploited to fulfil the irrigational water demands. Moreover, soils in Saudi Arabia are poor and lack tolerable drainage system. Harsh agricultural environments thrust the farmers to maximize daily groundwater pumpage to overcome the substantial daily evapotranspiration caused by the massive turbulent heat fluxes in the designated study area. Normalized difference salinity index was generated based on remotely sensed data derived from Landsat 8 acquired on April 14th, 2014, after proper radiometric and atmospheric corrections. Thematic map of soil salinity was generated and then reclassified into four classes based on the natural break classification techniques. On the other hand, fraction of absorbed photosynthetically active radiation (FAPAR) is another remotely sensed vegetation index established to envisage the effect of different soil salinity on the crop vigorously. FAPAR index was estimated using remote sensing data derived from the medium-spectral resolution imaging spectrometer on the same day of acquisition for consistency reasons. Results demonstrated that the FAPAR index is highly dependent on soil salinity. Higher soil salinity values corresponded to lower FAPAR values. Findings of the current research will help decision makers and decision takers to take soil salinity into consideration in future strategic plans.

Keywords: Crop vigorous; Efficiency; Environmental management; FAPAR; Soil salinity index; Remote sensing practices

1. Introduction

Water resources are limited and scarce in Saudi Arabia. The main source of freshwater is the groundwater [1]. During the last three decades we are witnesses of an extensive agricultural expansion to meet the domestic needs [2,3]. The expansion of the agricultural activities took place in different regions in Saudi Arabia. Primarily, it started in the central region of Saudi Arabia known as Al-Qassim [4,5].

Due to over exploitation of the groundwater to sustain the agricultural activities in Al-Qassim, the water table dropped dramatically to the extent of inability to pump up more groundwater [5]. Consequently, the agricultural activities in that region are mostly degraded and the agricultural activities moved in both of the northern (Al-Jouf) and the southern (Ad-Dawasir) regions of Saudi Arabia [1].

Saudi Arabia is characterized by arid climate conditions, extremely hot and long summer in addition to rare precipitations [6,7]. Aridity conditions drove the farmers to compensate the high evaporation rates by excessive irrigation to avoid cops welting [8]. The current groundwater pumpage regime led to additional natural resource degradation. Water logging and soil salinity augmentation are now the most limiting factors to the agricultural expansion in those areas [9,10].

The accumulation of salts in soils has radical effects on crop production. Salty soils compete with the crops on the

Presented at the 5th International Conference on Sustainable Solid Waste Management (ATHENS 2017), 21–24 June 2017, Athens, Greece.

available soil moisture content and make it unavailable for crops uptake [11]. Salts accumulation rapidly occurs in poorly drained soils, where the excess of the irrigational water stays on the top soils [12–14].

Remote sensing techniques are broadly used to overcome regional scale problems that directly related to crops production and its corresponding water demands [10,15–17]. There are several vegetation indices that are exercised to investigate soil/crop relationships [18,19]. Implementation of remote sensing data and geographic information systems (GIS) practices is reported in several scholarly works [20–23]. However, there is no ideal procedure to use remote sensing data in conjunction with GIS to examine soil/crop relationships [24,25].

Several soil salinity indices were developed to monitor the soil salinity levels in different ecosystems by using different satellite sensors [16,17]. The most exercised soil salinity index is the normalized difference salinity index (NDSI), due to the spectral bands availability in Landsat images [26].

Medium-spectral resolution imaging spectrometer (MERIS) is fairly used to estimate different vegetation indices [27]. The implemented algorithm utilizes top of atmosphere-vegetation (TOA-VEG) radiative transfer models and associated geometry as inputs [28,29]. The role of the adopted algorithm capitalizes the physical remote sensing measurements and discourses many operational limitations related to the systematic data analysis [30].

MERIS data can be used to generate fraction of absorbed photosynthetically active radiation (FAPAR). The latter is an important variable to distinguish crops drought condition [31,32]. FAPAR principally depends on visible/near infrared spectral bands of MERIS data. These bands are rectified to ensure their prime atmospheric decontamination as well as the removal of any angular effects [28,32,33].

TOA reflectance simulation using MERIS spectral bands (13 spectral bands) necessitates 15 different input variables based on the experimental design to ensure the realization of equal canopy occupied spaces [31,34]. Generally, there is no wide agreement on specific measures to estimate FAPAR taken into consideration the environmental conditions and a certain input data sets [32,35,36].

The aim of the current study is to envisage the effect of different soil salinity levels in correspondence to remotely sensed FAPAR index as an indicator of water stress condition in Wadi Ad-Dawasir.

2. Materials and method

2.1. Study area

The study area is located in Najd plateau at 20°27′52″N 044°47′14″E. It is characterized by gravelly tableland disconnected by insignificant sandy oases and isolated mountain bundles (Fig. 1). The tableland descends toward the east from an elevation of 1,360 m (4,462 ft) in the west to 750 m (2,460 ft) at its easternmost limit. The major source of irrigational water in Wadi Ad-Dawasir is the abstraction from Al-Wajid aquifer. Agriculture in Wadi Ad-Dawasir area consists of technically highly developed farm enterprises that operate modern pivot irrigation system. The size of center pivot ranges from 30 to 60 ha (75–149 acr) with farmers managing hundreds of them including the corresponding number of wells. The main crop grown in winter is wheat (*Triticum aestivum*) and occasionally potatoes (*Solanum tuberosum* L.), tomatoes (*Solanum lycopersicum*) or melons (*Citrullus lanatus*). All year fodder consists of alfalfa (*Medicago sativa*), which is cut up to 10 times a year for animal feed. Typical summer crops for fodder are sorghum (*Sorghum bicolor*) and Rhodes grass (*Chloris gayana*), which is perennial, but dormant in winter. The shallow alluvial aquifers could not sustain the high groundwater abstraction rates for a long time and groundwater level declined dramatically in most areas [5]. Meteorological features of the area are speckled. Five elements of meteorology are constantly recorded with fixed weather station located within the study area. Temperature varies from 6°C as minimum temperature to 43°C as maximum temperature. The relative humidity is mostly stable at 24%. Solar radiation (W/m^2) of average sunrise duration is 11 h/d. Average wind speed is closer to 13 km/h and may reach up to 46 km/h in thunderstorm incidents. Finally, mean annual rainfall is about 37.6 mm [37].

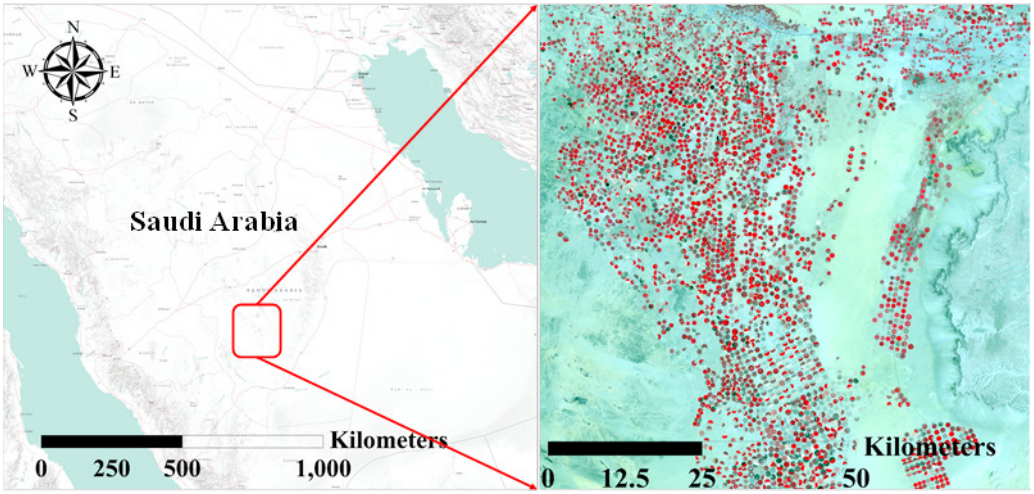

Fig. 1. Location of the study area.

2.2. Methodological framework

The current research work is based on assessing the efficiency correlation between estimated FAPAR corresponding salinity index (SI's) values obtained from satellite images. Therefore, field data collection was carried out with accurate synchronization of satellite bypassing over the designated study area to avoid any atmospheric discrepancies.

2.2.1. Soil sampling and analysis

A total number of 150 random soil samples were collected based on simple random sampling technique from Wadi Ad-Dawasir area with a minimum distance of 100 m (329ft) between the samples location to avoid data clumping (Fig. 2). The standard procedure for determining soil extract salinity in terms of electrical conductivity was followed according to Shaw [38] under laboratory condition.

2.2.2. Remote sensing data

In the current study, two different satellite sensors were used Landsat 8 and MERIS. Landsat 8 scene was acquired on April 17th, 2014. Fundamental radiometric and atmospheric corrections were applied to visible and near infrared bands according to Chavez [40] and Beisl et al. [41]. Moreover, MERIS scene was also acquired on the same date of Landsat acquisition to minimize the atmospheric variations between the two scenes. MERIS sensor has a spatial resolution of 300 m at nadir designed to acquire data over the Earth whenever illumination conditions are suitable [42]. MERIS sensor was designed to derive estimates of the concentration of chlorophyll-a. Therefore, MERIS data are very important to monitor photosynthesis process based on the effective estimation of solar radiation fraction consumed by crops [14,43].

Landsat 8 images are consisting of nine spectral bands ranging from visible to thermal infrared with a spatial resolution of 30 m for bands from 1 to 7 and then 9. The resolution for the panchromatic band 8 is 15 m. Spectral bands are selectable across the range of 435–1,251 nm. Meanwhile, MERIS land and coast images are consisted of 15 spectral bands ranging from visible to near infrared with spatial resolution of 300 m. Spectral bands are selectable across the range of 390–1,040 nm.

2.2.3. Estimation of remote sensing indices

NDSI and FAPAR were estimated individually using corresponding remote sensing data according to the following equations.

- NDSI is estimated according to Major et al. [26] as follows:

$$NDSI = (R - NIR)/(R + NIR) \quad (1)$$

where R is red band of Landsat 8; NIR is near infrared band of Landsat 8.

- FAPAR is estimated according to Gobron et al. [44] and Vermote et al. [45] as follows:

$$\tilde{\rho}(\lambda_i) = \frac{\rho^{TOA}(\Omega_0, \Omega_v, \lambda_i)}{F(\Omega_0, \Omega_v, k_{\lambda i}, \Omega_{\lambda i}^{HG}, \rho_{\lambda ic})} \quad (2)$$

where λ_i is the wavelength (blue, red or near-infrared) of spectral band i, $\rho^{TOA}(\Omega_0, \Omega_v, \lambda_i)$ is the bidirectional reflectance factor values measured by the sensor in the spectral band λ_i, Ω_0 is the actual geometry of illumination; Ω_v is the actual geometry of observation; $F(\Omega_0, \Omega_v, k_{\lambda i}, \Omega_{\lambda i}^{HG}, \rho_{\lambda ic})$ is the shape of the radiance field; $k_{\lambda i}$, $\Omega_{\lambda i}^{HG}$, $\rho_{\lambda ic}$ is the Rahman-Pinty-Verstraete parameters according to Rahman et al. [46].

Red and infrared MERIS spectral bands require radiometric correction. Radiometric correction processed as follows:

$$\rho_{Rred} = g1\left[\tilde{\rho}(\lambda_{blu}), \tilde{\rho}(\lambda_{red})\right] \quad (3)$$

$$\rho_{Rnir} = g2\left[\tilde{\rho}(\lambda_{blu}), \tilde{\rho}(\lambda_{nir})\right] \quad (4)$$

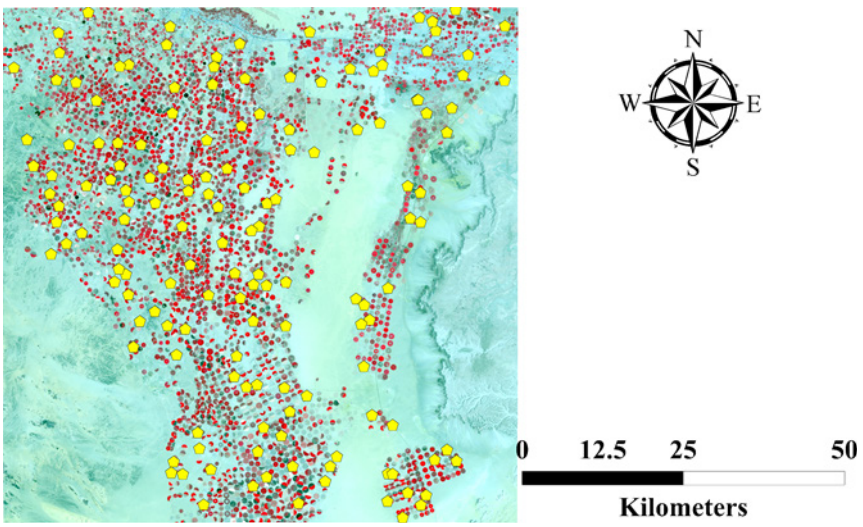

Fig. 2. Soil sample location on a false color composite of Landsat 8 image [39].

Meanwhile,

$$gn\left[\tilde{\rho}\left(\lambda_{\text{blu}}\right),\tilde{\rho}\left(\lambda_{\text{red}}\right)\right]=\frac{P\left(\lambda_i,\lambda_j\right)}{Q\left(\lambda_i,\lambda_j\right)} \tag{5}$$

$$P\left(\lambda_i,\lambda_j\right)=l_{n,1}\left(\tilde{\rho}\left(\lambda_i\right)+l_{n,2}\right)^2+l_{n,3}\left(\tilde{\rho}\left(\lambda_j\right)+l_{n,4}\right)^2+l_{n,5}\tilde{\rho}\left(\lambda_i\right)\tilde{\rho}\left(\lambda_j\right) \tag{6}$$

$$Q\left(\lambda_i,\lambda_j\right)=l_{n,6}\left(\tilde{\rho}\left(\lambda_i\right)+l_{n,7}\right)^2+l_{n,8}\left(\tilde{\rho}\left(\lambda_j\right)+l_{n,9}\right)^2+l_{n,10}\tilde{\rho}\left(\lambda_i\right)\tilde{\rho}\left(\lambda_j\right)+l_{n,11} \tag{7}$$

The optimization of the polynomial coefficients $l_{n,m}$ was carried out based on the normalization of each bi-directional reflectance and its corresponded spectral polynomial values of $g_n[\tilde{\rho}(\lambda_{\text{blu}}), \tilde{\rho}(\lambda_j)]$ under anisotropic reflectance function [33,47]. Corrected channels used to estimate FAPAR as follows:

$$g0=\left(\rho_{\text{Rred}},\rho_{\text{Rnir}}\right)=\frac{l_{0,1}\rho_{\text{Rnir}}-l_{0,2}\rho_{\text{Rred}}-l_{0,3}}{\left(l_{0,4}-\rho_{\text{Rred}}\right)^2+\left(l_{0,5}-\rho_{\text{Rnir}}\right)^2+l_{0,6}} \tag{8}$$

2.2.4. Regression analysis

The regression analysis is the practice of creating a curve, or mathematical function that has the best fit to a series of data points, possibly subject to constraints. There are several fitting functions and there is no general best fit. Best fit is a data dimension and mathematical function dependent [48–51].

In this study, the neural analysis [52] and multivariate analysis [53] were applied to examine the relationship between FAPAR and NDSI. The neural network regression model is written as:

$$Y=\alpha+\Sigma_h w_h\phi_h(\alpha_h+\Sigma_{i=1}^{p}w_{ih}X_i) \tag{9}$$

where $Y = E(Y|X)$. This neural network model has one hidden layer, but it is possible to have additional hidden layers. The $\phi(z)$ function used is hyperbolic tangent activation function. It is used for logistic activation for the hidden layers.

$$\phi\left(z\right)=\tanh\left(z\right)=\frac{1-e^{-2z}}{1+e^{-2z}} \tag{10}$$

It is significant that the final outputs to be linear not to constrain the predictions to be between 0 and 1. The equation for the skip-layer neural network for regression is shown below:

$$Y=\alpha+\Sigma_{i=1}^{p}\beta_i X_i+\Sigma_h w_h\phi_h(\alpha_h+\Sigma_{i=1}^{p}w_{ih}X_i) \tag{11}$$

It should be clear that these models are highly parameterized and thus will tend to over fit the training data. Cross-validation is therefore critical to make sure that the predictive performance of the neural network model is adequate. Recall the skip-layer neural network regression model looks like this:

$$Y=\alpha+\Sigma_{i=1}^{p}\beta_i X_i+\Sigma_h w_h\phi_h(\alpha_h+\Sigma_{i=1}^{p}w_{ih}X_i) \tag{12}$$

However, this model most likely overfits the training data. Consequently, determination of the adequate performance of the artificial neural networks model is a must. Five different criteria are used: the Pearson coefficient of correlation (*R*), the root mean square error (RMSE), the mean absolute deviation, the negative log-likelihood and the unconditional sum of squares. Basically, RMSE is the examined parameter for comparability reasons. RMSE can be computed as:

$$\text{RMSE}=\sqrt{\frac{1}{T_0}\Sigma_{t=1}^{T_0}\left(y_1-\acute{y}_1\right)^2} \tag{13}$$

where *t* is the time index, and *y*ˆ*t* and *yt* are the simulated and measured values. Principally, the higher value of *R* and smaller values of RMSE ensure the better performance of model.

2.2.5. Correspondence analysis

Correspondence analysis was carried in order to assess the current agricultural practice in the designated study area. Correspondence analysis involves estimation of average accuracy, average reliability and overall efficiency. The average accuracy is estimated by a horizontal function of the tested dataset. The average reliability is estimated by a vertical function of the tested dataset. The overall efficiency is estimated the diagonal function of the tested dataset. Following Congalton and Mead [54], a correspondence analysis was constructed as follows:

$$\text{CA}=\frac{N\Sigma_{i=1}^{r}x_{ii}-\Sigma_{i=1}^{r}\left(x_{ij}\times x_{ji}\right)}{N^2-\Sigma_{i=1}^{r}\left(x_{ij}\times x_{ji}\right)} \tag{14}$$

where *r* is the number of rows in the error matrix; x_{ii} is the number of observations in row *i* and column *i* (the diagonal cells); x_{i+} is the total observations of row *i*; x_{+I} is the total observations of column *i*; and *N* is the total of observations in the matrix.

2.3. Validation

Validation of NDSI values was carried out using the ground truth data collection. 150 soil samples were analyzed for electric conductivity measured in ppm and plotted against the remotely sensed salinity values. Validation of FAPAR values was carried by according to Gobron et al. [31,55] using different canopy radiation transfer regimes under European Joint Research Centre (JRC) utilizing sea-viewing wide field-of-view sensor plotted against ground truth data.

3. Results and discussion

The adopted methodology resulted in two different thematic maps, soil salinity map (Fig. 3) and FAPAR index map (Fig. 4). The two maps were then reclassified into four classes according to natural break classification [56].

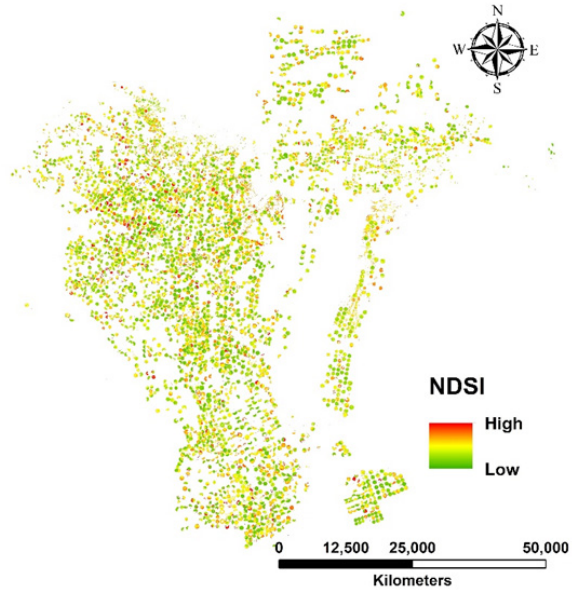

Fig. 3. NDSI spatial distribution in Wadi Ad-Dawasir.

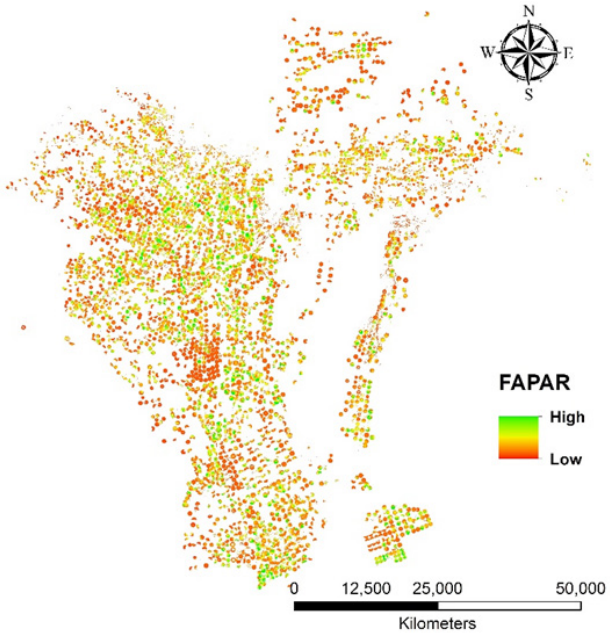

Fig. 4. FAPAR spatial distribution in Wadi Ad-Dawasir.

Soil salinity spatial variation demonstrates that the peripheral areas of Wadi Ad-Dawasir agriculture areas are highly salinized, especially the new agricultural expansion at the southern west part of the designated study area [39]. This could be explained by the fact that the study area is characterized by affluence relief. Therefore, the sprinkle movement drove the accumulation of excess waters at the peripherals of the agricultural areas [24,57].

Evaluation of estimated NSDI values using remote sensing data was plotted against ground truth data collected from 150 soil samples demonstrated in Fig. 5. The robust correlation was noticed at R^2 value of 0.97 [10,39].

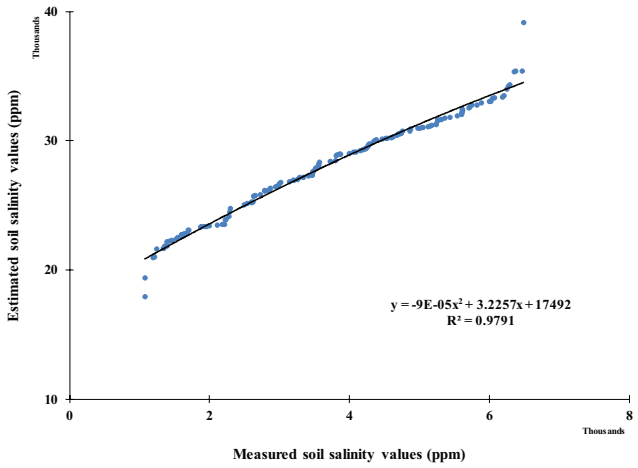

Fig. 5. Regression analysis between measured and estimated soil salinity values.

Spatial variations of FAPAR values followed a similar pattern of NDSI values. The lower FAPAR values were located at the newly agricultural expansion (southern west part of the designated study area). This could be explained by the less availability of soil moisture content to crops. Due to salt accumulation in soils, there is no enough available water in soils for proper photosynthesis process [17,24].

According to Table 1, the polynomial fit was the best to describe the relationship between NDSI and FAPAR to be read as FAPAR = 0.6326351 – 6.4654e–6 × NDSI + 8.66e–10 × (NDSI – 42468)^2. The RMSE was expressed its lowest value among the other regression models at the polynomial fit [58]. Regardless the outliers, the NDSI cloud data were centralized around 5,000 ppm of salt and its corresponding FAPAR value of 0.1 as it demonstrated in Fig. 6. This co-occurrence indecently proves that higher soil salinity values affect drastically the photosynthesis process, particularly in arid environments [11,19].

Quantification of the current agricultural practice efficiency was assessed by the confusion matrix. System accuracy and reliability were calculated in Table 2 while overall efficiency was calculated in Table 3 to be 49.54%.

RMSE is explicitly defining the deviated predictions, on average, from the actual values. While R^2 is conveniently scaled between 0 and 1. Obviously R^2 can be more easily interpreted, but RMSE is more accurate because it is not scaled to any particular values [59].

The reclassification method used in the current study assigned four ordinal values to the resulted thematic maps according to their intensities ranges from high stability (rank 4) to no suitability (rank 1). Subsequently, NDSI and FAPAR thematic maps were converted into vector files using the ordinal ranking. Consequently, intersection function under GIS environment was applied and the resulted matrix is shown in Table 3. According to the matrix, the system efficiency is calculated to be 49% (the diagonal sum over the total sum). This clearly stated that the agricultural practice in Wadi Ad-Dawasir needs to be comprehensively reviewed in term of water saving strategies and the horizontal expansion if the newly reclaimed land [2,10].

Table 1
Statistical evaluations of NDSI and FAPAR paramount fitting

	Polynomial fit	Linear fit	Sigmoidal fit	Gaussian fit
R^2	0.163383	0.138729	0.149331	0.14738
R^2 adj.	0.152	0.13291	0.098181	0.098406
Root mean square error	**0.31074**	0.314218	0.313339	0.313698
Mean of response	0.435548	0.435548	0.435548	0.435548
Observations (or sum weights)	150	150	150	150

Bold number represent the best fit.

Table 2
Agricultural practice in Wadi Ad-Dawasir accuracy and reliability

Accuracy (%)	FAPAR classes				Reliability (%)	FAPAR classes			
NDSI classes	65.27	26.11	5.83	2.80	NDSI classes	99.75	37.18	6.75	8.22
	0.17	8.74	91.09	0.00		0.14	6.97	59.16	0.01
	0.12	54.67	40.35	4.88		0.11	55.78	33.50	10.27
	0.00	0.16	1.81	98.01		0.00	0.07	0.59	81.50

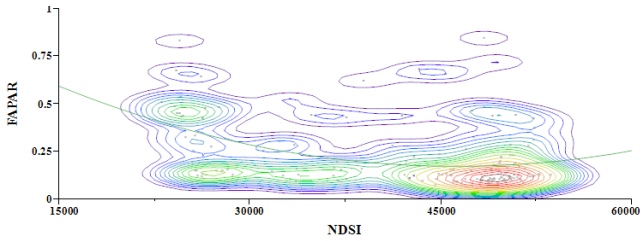

Fig. 6. Neural network analysis of NDSI (ppm) and FAPAR (dimensionless).

Table 3
Confusion matrix of Wadi Ad-Dawasir agricultural practice suitability

	FAPAR "suitability from high to low" →				Total (km²)
NDSI "suitability from high to low" ↓	**280**	112	25	12	429
	0.4	**21**	219	0.01	240.41
	0.3	168	**124**	15	307.3
	0.01	0.2	2.2	**119**	121.41
Total (km²)	280.71	301.2	370.2	146.01	**1,098.12**

Bold numbers represent the diagonal of the matrix.

4. Conclusion

The groundwater resources are the only water source of irrigation to sustain the agricultural activities taken place in Wadi Ad-Dawasir. Moreover, the designated study area soils are poorly drained although the pumpage rates are higher than the actual crop needs. Horizontal expansions of the agricultural areas are the driving forces of underground water resources over exploitation, regardless the physical and chemical properties of the utilized soils. Remote sensing techniques in terms of vegetation indices were fairly exercised in the current study and present reliable assessment of the current agricultural practice in the area. NDSI and FAPAR showed no discrepancies in interpretation of the salinity problem conjunction with low photosynthetic capabilities. The current study strongly suggests decision makers and decision takers to review the existing agricultural strategy in Wadi Ad-Dawasir. Rational groundwater resources utilization and crop allocation needs to be taken into consideration. Meanwhile, soil physical and chemical properties need to be thoroughly investigated along with temporal monitoring of the designated area soils.

Acknowledgments

This work was supported by the Deanship of Scientific Research (DSR) at King Abdulaziz University, Jeddah, under grant no. 006-155-1438D. The authors, therefore, gratefully acknowledge the DSR for technical and financial support.

References

[1] S. Chowdhury, M. Al-Zahrani, Characterizing water resources and trends of sector wise water consumptions in Saudi Arabia, J. King Saud Univ. Eng. Sci., 27 (2015) 68–82.
[2] W.A. Abderrahman, Water demand management in Saudi Arabia, Water Manage., 1 (2001) 61.
[3] M. Ahmed, S. Al-Jabri, B. Choudri, M. Raouf, M. Luomi, Green Challenges and Some Technological Solutions in the Water Sector of the Gulf Cooperation Council Countries, The Green Economy in the Gulf, Routledge, Abingdon, 2015, p. 123.
[4] K.H. Al-Zahrani, Water demand management in the Kingdom of Saudi Arabia, in Conference of the International Journal of Arts & Sciences, 2010.
[5] K.H. Al-Zahrani, M.B. Baig, Water in the Kingdom of Saudi Arabia: sustainable management options, J. Anim. Plant Sci., 21 (2011) 601–604.
[6] M. Elhag, J.A. Bahrawi, Conservational use of remote sensing techniques for a novel rainwater harvesting in arid environment, Environ. Earth Sci., 72 (2014) 4995–5005.
[7] M. Elhag, J.A. Bahrawi, Potential rainwater harvesting improvement using advanced remote sensing applications, Sci. World J., 2014 (2014) 1–8.

[8] J.M. Bradd, W.A. Milne-Home, G. Gates, Overview of factors leading to dryland salinity and its potential hazard in New South Wales, Australia, Hydrogeol. J., 5 (1997) 51–67.
[9] E. Houk, M. Frasier, E. Schuck, The agricultural impacts of irrigation induced waterlogging and soil salinity in the Arkansas Basin, Agric. Water Manage., 85 (2006) 175–183.
[10] M. Elhag, Evaluation of different soil salinity mapping using remote sensing techniques in arid ecosystems, Saudi Arabia, J. Sens., 2016 (2016) 1–8.
[11] R. Jones, G. Marshall, Land salinisation, waterlogging and the agricultural benefits of a surface drainage scheme in Benerembah irrigation district, Rev. Market. Agric. Econ., 60 (1992) 173–189.
[12] D. Williamson, Land Degradation Processes and Water Quality Effects, Water Logging and Salinity, Farming Action-Catchment Reaction, the Effect of Dry-Land Farming on the Natural Environment, CSIRO Publishing, Collingwood, VIC, 1998, pp. 162–190.
[13] S. Abdel-Dayem, S. Abdel-Gawad, H. Fahmy, Drainage in Egypt: a story of determination, continuity, and success, Irrig. Drain., 56 (2007) S101–S111.
[14] M. Elhag, J.A. Bahrawi, Realization of daily evapotranspiration in arid ecosystems based on remote sensing techniques, Geosci. Instrum. Methods Data Syst., 6 (2017) 141.
[15] L. Montandon, E. Small, The impact of soil reflectance on the quantification of the green vegetation fraction from NDVI, Remote Sens. Environ., 112 (2008) 1835–1845.
[16] B.D. Wardlow, S.L. Egbert, Large-area crop mapping using time-series MODIS 250 m NDVI data: an assessment for the US Central Great Plains, Remote Sens. Environ., 112 (2008) 1096–1116.
[17] Z. Yang, J. Gao, C. Zhou, P. Shi, L. Zhao, W. Shen, H. Ouyang, Spatio-temporal changes of NDVI and its relation with climatic variables in the source regions of the Yangtze and Yellow rivers, J. Geog. Sci., 21 (2011) 979–993.
[18] A.E.K. Douaoui, H. Nicolas, C. Walter, Detecting salinity hazards within a semiarid context by means of combining soil and remote-sensing data, Geoderma, 134 (2006) 217–230.
[19] G. Jiapaer, X. Chen, A. Bao, A comparison of methods for estimating fractional vegetation cover in arid regions, Agric. For. Meteorol., 151 (2011) 1698–1710.
[20] B. Rao, R. Dwivedi, L. Venkataratnam, T. Ravishankar, S. Thammappa, G. Bhargawa, A. Singh, Mapping the magnitude of sodicity in part of the Indo-Gangetic plains of Uttar Pradesh, Northern India using Landsat-TM data, Int. J. Remote Sens., 12 (1991) 419–425.
[21] A. Srivastava, N. Tripathi, K. Gokhale, Mapping groundwater salinity using IRS-1B LISS II data and GIS techniques, Int. J. Remote Sens., 18 (1997) 2853–2862.
[22] R. Dwivedi, K. Sreenivas, Delineation of salt-affected soils and waterlogged areas in the Indo-Gangetic plains using IRS-1C LISS-III data, Int. J. Remote Sens., 19 (1998) 2739–2751.
[23] A. Psilovikos, M. Elhag, Forecasting of remotely sensed daily evapotranspiration data over Nile Delta region, Egypt, Water Resour. Manage., 27 (2013) 4115–4130.
[24] R.S. Lunetta, J. Ediriwickrema, D.M. Johnson, J.G. Lyon, A. McKerrow, Impacts of vegetation dynamics on the identification of land-cover change in a biologically complex community in North Carolina, USA, Remote Sens. Environ., 82 (2002) 258–270.
[25] X. Zhan, R. Sohlberg, J. Townshend, C. DiMiceli, M. Carroll, J. Eastman, M. Hansen, R. DeFries, Detection of land cover changes using MODIS 250 m data, Remote Sens. Environ., 83 (2002) 336–350.
[26] D. Major, F. Baret, G. Guyot, A ratio vegetation index adjusted for soil brightness, Int. J. Remote Sens., 11 (1990) 727–740.
[27] M. Elhag, Remotely sensed vegetation indices and spatial decision support system for better water consumption Regime in Nile Delta. A case study for rice cultivation suitability map, Life Sci. J., 11 (2014) 201–209.
[28] N. Gobron, B. Pinty, M.M. Verstraete, J.-L. Widlowski, Advanced vegetation indices optimized for up-coming sensors: design, performance, and applications, IEEE Trans. Geosci. Remote Sens., 38 (2000) 2489–2505.
[29] F. Baret, O. Hagolle, B. Geiger, P. Bicheron, B. Miras, M. Huc, B. Berthelot, F. Niño, M. Weiss, O. Samain, LAI, fAPAR and fCover CYCLOPES global products derived from VEGETATION: Part 1: principles of the algorithm, Remote Sens. Environ., 110 (2007) 275–286.
[30] I. McCallum, W. Wagner, C. Schmullius, A. Shvidenko, M. Obersteiner, S. Fritz, S. Nilsson, Comparison of four global FAPAR datasets over Northern Eurasia for the year 2000, Remote Sens. Environ.,. 114 (2010) 941–949.
[31] N. Gobron, O. Aussedat, B. Pinty, MODerate Resolution Imaging Spectroradiometer, JRC-FAPAR Algorithm Theoretical Basis Document, EUR Report No. 22164 EN, 2006.
[32] N. Gobron, B. Pinty, O. Aussedat, M. Taberner, O. Faber, F. Mélin, T. Lavergne, M. Robustelli, P. Snoeij, Uncertainty estimates for the FAPAR operational products derived from MERIS—impact of top-of-atmosphere radiance uncertainties and validation with field data, Remote Sens. Environ., 112 (2008) 1871–1883.
[33] N. Gobron, B. Pinty, M. Verstraete, M. Taberneret, VEGETATION, An optimized FAPAR Algorithm Theoretical Basis Document, Publications Office of the European Union, Luxembourg, UK, JRC Publications, Europe, Vol. 20146, 2002.
[34] J. Hu, Y. Su, B. Tan, D. Huang, W. Yang, M. Schull, M.A. Bull, J.V. Martonchik, D.J. Diner, Y. Knyazikhin, Analysis of the MISR LAI/FPAR product for spatial and temporal coverage, accuracy and consistency, Remote Sens. Environ., 107 (2007) 334–347.
[35] K. Huemmrich, J. Privette, M. Mukelabai, R. Myneni, Y. Knyazikhin, Time-series validation of MODIS land biophysical products in a Kalahari woodland, Africa, Int. J. Remote Sens., 26 (2005) 4381–4398.
[36] M. Jung, M. Verstraete, N. Gobron, M. Reichstein, D. Papale, A. Bondeau, M. Robustelli, B. Pinty, Diagnostic assessment of European gross primary production, Global Change Biol., 14 (2008) 2349–2364.
[37] M. Elhag, J. Bahrawi, Cloud coverage disruption for groundwater recharge improvement using remote sensing techniques in Asir Region Saudi Arabia, Life Sci. J., 11 (2014) 192–200.
[38] R.J. Shaw, Estimation of the Electrical Conductivity of Saturation Extracts from the Electrical Conductivity of 1:5 soil: Water Suspensions and Various Soil Properties, Department of Primary Industries Queensland, 1994.
[39] M. Elhag, J.A. Bahrawi, Soil salinity mapping and hydrological drought indices assessment in arid environments based on remote sensing techniques, Geosci. Instrum. Methods Data Syst., 6 (2017) 149.
[40] P.S. Chavez, Image-based atmospheric corrections-revisited and improved, Photogramm. Eng. Remote Sens., 62 (1996) 1025–1035.
[41] U. Beisl, J. Telaar, M. Schönermark, Atmospheric correction, reflectance calibration and BRDF correction for ADS40 image data, Int. Arch. Photogramm. Remote Sens. Spat. Info. Sci., 37 (2008) 7–12.
[42] J. Huot, M. Rast, S. Delwart, J. Bezy, G. Levrini, H. Tait, The optical imaging instruments and their applications: AATSR and MERIS, ESA Bull., 106 (2001) 56–66.
[43] B. Pinty, T. Lavergne, M. Voßbeck, T. Kaminski, O. Aussedat, R. Giering, N. Gobron, M. Taberner, M. Verstraete, J.L. Widlowski, Retrieving surface parameters for climate models from moderate resolution imaging spectroradiometer (MODIS)-multiangle imaging spectroradiometer (MISR) albedo products, J. Geophys. Res. Atmos., 112 (2007) (D10).
[44] N. Gobron, B. Pinty, M.M. Verstraete, Y. Govaerts, A semidiscrete model for the scattering of light by vegetation, J. Geophys. Res. Atmos., 102 (1997) 9431–9446.
[45] E.F. Vermote, D. Tanré, J.L. Deuze, M. Herman, J.-J. Morcette, Second simulation of the satellite signal in the solar spectrum, 6S: an overview, IEEE Trans. Geosci. Remote Sens., 35 (1997) 675–686.
[46] H. Rahman, B. Pinty, M.M. Verstraete, Coupled surface-atmosphere reflectance (CSAR) model: 2. Semiempirical surface model usable with NOAA advanced very high resolution radiometer data, J. Geophys. Res. Atmos., 98 (1993) 20791–20801.

[47] N. Gobron, B. Pinty, M. Verstraete, M. Taberner, Global Land Imager (GLI) An optimized FAPAR Algorithm Theoretical Basis Document, Joint Research Centre, Institute for Environment and Sustainability, Publication no.: EUR 20147 EN, 2002.
[48] T.J. Hastie, R.J. Tibshirani, Generalized Additive Models, CRC Press, Florida, USA, 43 (1990).
[49] J. Chambers, W. Cleveland, B. Kleiner, P. Tukey, Graphical Methods for Data Analysis, Duxbury Press, Massachusetts, USA, Boston, 1983.
[50] W. Press, S. Teukolsky, W. Vetterling, B. Flannery, Numerical Recipes, Cambridge University Press, New York, NY, 1992.
[51] E.A. McBean, F.A. Rovers, Statistical Procedures for Analysis of Environmental Monitoring Data and Risk Assessment, Prentice Hall PTR, New Jersey, USA, 1998.
[52] J.C. Hsu, Constrained simultaneous confidence intervals for multiple comparisons with the best, Ann. Stat., 12 (1984) 1136–1144.
[53] T. Anderson, An Introduction to Multivariate Statistical Analysis, Wiley, NY, 1984.
[54] R. Congalton, R.A. Mead, A quantitative method to test for consistency and correctness in photointerpretation, Photogramm. Eng. Remote Sens., 49 (1983) 69–74.
[55] N. Gobron, B. Pinty, O. Aussedat, J. Chen, W.B. Cohen, R. Fensholt, V. Gond, K.F. Huemmrich, T. Lavergne, F. Mélin, Evaluation FAPAR products for different canopy radiation transfer regimes: methodology and results using JRC products derived from SeaWiFS against ground-based estimations, J. Geophys. Res., 111 (2006) p. D13110.
[56] G.F. Jenks, Generalization in statistical mapping, Ann. Assoc. Am. Geogr., 53 (1963) 15–26.
[57] F. Konukcu, J. Gowing, D. Rose, Dry drainage: a sustainable solution to waterlogging and salinity problems in irrigation areas?, Agric. Water Manage., 83 (2006) 1–12.
[58] B. Jiang, Head/tail breaks: a new classification scheme for data with a heavy-tailed distribution, Prof. Geogr., 65 (2013) 482–494.
[59] T. Chai, R.R. Draxler, Root mean square error (RMSE) or mean absolute error (MAE)? – arguments against avoiding RMSE in the literature, Geosci. Model Dev., 7 (2014) 1247–1250.